Eur. Phys. J. A **11**, 155–160 (2001)

THE EUROPEAN PHYSICAL JOURNAL A

Thick skin in neutron/proton-rich sodium isotopes

Y.K. Gambhir[1,a], A. Bhagwat[1], N. Van Giai[2], and P. Schuck[2]

[1] Indian Institute of Technology, Powai, Mumbai 400076, India
[2] Institut de Physique Nucléaire, Université Paris-Sud, F-91406 Orsay Cedex, France

Received: 24 April 2001 / Revised version: 14 June 2001
Communicated by Th. Walcher

Abstract. Nucleon (both neutron and proton) density distributions of the chain of sodium isotopes are calculated using a semi-phenomenological model of nuclear density which incorporates correctly the asymptotic behaviour and the behaviour near the centre. The experimental charge root-mean-square radii and the single neutron and proton separation energies, required as input, are used. The calculated interaction cross-sections using these densities in the Glauber model agree well with the experiment. The calculated neutron rms radii $r_{\rm n}$ and the nuclear skin thickness $(r_{\rm n} - r_{\rm p})$ closely agree with the corresponding experimental values and also are consistent with the Relativistic Hartree-Bogoliubov (RHB) calculations.

PACS. 27.20.+n $6 \leq A \leq 19$ – 21.10.Ft Charge distribution – 21.60.-n Nuclear-structure models and methods – 25.70.-z Low and intermediate energy heavy-ion reactions

1 Introduction

The fragmentation process in the present day heavy-ion collision experiments helps to produce a variety of exotic nuclei. These may have large neutron/proton excess, usually have small nucleon separation energy and may even lie close to the drip line. The radioactive ion beam (RIB) facility helps to separate and accelerate such a particular exotic nuclear beam, which in turn can be used as a secondary beam for further experimental studies. This then allows to study highly unstable nuclei which otherwise would have been difficult. Such studies have already revealed a new rich variety of phenomena, like neutron/proton halos, thick neutron skin, etc. (*e.g.*, see [1,2]).

Nucleon (neutron/proton) distributions inside a nucleus are one of the fundamental properties of nuclei dictated by the interaction between the nucleons in the medium. Conventionally, extremely accurate information about the charge distribution (*i.e.*, the folded proton density distribution) of stable nuclei was and is being obtained through electron scattering experiments. On the other hand, such experimental information of comparable precision on neutron density distribution is, however, not available though acceptable information on differences in radii of neutron and proton density distributions have been obtained [3].

The study of loosely bound nuclei is of current interest and several such studies have been/are being reported. One of the aims is to extract the information about neutron density distributions in such exotic nuclei. For this purpose, one uses the Glauber model. The Glauber model requires the proton and neutron density distributions of both the target and the projectile. If the target density distribution is reasonably known then the neutron density distribution of the projectile can be extracted knowing its proton distribution. In fact it has been possible to reproduce the observed cross-sections in the Glauber model by fitting parameter(s) appearing in a reasonably assumed form for the neutron density distribution of the projectile (exotic nucleus), *e.g.*, the harmonic oscillator (HO) form [1,4]. Such an analysis may give reliable information about the size of the nucleus, but may not determine correctly the shape of the density distribution. Explicitly, for example, in the case of ^{11}Li, the core (^{9}Li) density was taken to be of HO type and the halo neutrons were assumed to move independently in the average potential provided by the core with the same shape as that of the core density. The depth and the width of this potential were treated as parameters which were determined so as to give the right neutron separation energy (asymptotic behaviour) and a resulting density which in the Glauber model, yields the overall best fit to the experimental reaction cross-sections [5]. This is the present scenario and the densities thus extracted are termed as the experimental neutron densities.

Theoretically, the mean-field calculations are believed to give the most reliable nucleon density distributions. The non relativistic (the Density-Dependent Hartree-Fock (DDHF) with Skyrme-type interactions) approach and

[a] e-mail: yogy@phy.iitb.ac.in

its relativistic counterpart (the Relativistic Mean Field (RMF) or the Relativistic Hartree-Bogoliubov (RHB)) are being employed for such studies. These mean-field calculations do not automatically guarantee the correct prediction of the single nucleon separation energy, as a result, the asymptotic behaviour of the nuclear density distribution may not be well reproduced. On the other hand, in these loosely bound nuclei, the separation energy is small and the tail part of the density distribution may become crucial in the description of their properties. For this purpose, a semi-phenomenological model has been proposed [6] and has been successfully used for the description of loosely bound isotopes of He, Li, Be and B [7,8].

As mentioned earlier, nuclear sizes are one of the fundamental properties of the nuclei. The chain of sodium isotopes is a rare example of isotopic chain which has been investigated both experimentally and theoretically. Isotopic shift measurements have been reported [9] for this chain of isotopes. The knowledge of the charge radius of the stable sodium isotope, ^{23}Na, then yields the charge radii of the remaining isotopes. Recently, the same chain of isotopes has been studied using the RIB technique and, knowing the respective proton density distributions, the corresponding neutron density distributions have been extracted [10]. Theoretically also mean-field calculations have become available [11–13]. Perhaps one of the most interesting features of this problem is the stringent constraint imposed on the isospin channel of the nucleon-nucleon interaction. Thus, it is very interesting to investigate this chain of isotopes using also the semi-phenomenological density [6,8]. Here, we report the results obtained with the semi-phenomenological density distributions and compare these with the corresponding results of the microscopic RHB approach and the experiment.

The model density is discussed briefly in sect. 2. The results of the calculations using the semi-phenomenological density are presented, discussed and compared with the corresponding results of the RHB calculations and also with the experimental results wherever available in sect. 3. Cconcluding remarks are contained in the last section.

2 The model

A semi-phenomenological model for the nucleon density distributions of nuclei near the β stability line was proposed incorporating correctly two physical requirements [6]:

- behaviour near the centre ($r \to 0$),
- asymptotic behaviour ($r \to \infty$).

The first requirement demands that all derivatives of the density exist at the centre. This, in turn, requires that the power series expansion of $\rho(r)$ should contain only even powers of r. On the other hand, the "correct" asymptotic behaviour is given by [6]

$$\rho_i(r) \longrightarrow r^{-2\beta_i} e^{-r/a_i}, \tag{1}$$

where

$$a_i = \frac{\hbar}{2(2m\varepsilon_i)^{1/2}} \tag{2}$$

and

$$\beta_i = q\alpha \left(\frac{mc^2}{2\varepsilon_i}\right)^{1/2} + 1; \tag{3}$$

$\alpha = e^2/(4\pi\epsilon_0)\hbar c$, i = n or p, ε_i is the corresponding nucleon separation energy, $q = 0$ for neutrons and $q = Z - 1$ for protons, Z being the atomic number, and m is the reduced mass which, for simplicity, is taken as the nucleon mass. It is to be pointed out that, due to the Coulomb interaction, the asymptotic behaviour (eq. (1)) is different (through the charge q) for neutrons and protons. The model successfully reproduces the sizes (neutron and matter root-mean-square (rms) radii) [14] and electron scattering form factors [15] of series of nuclei near the β stability line. The model has been extended [7,8] to the description of loosely bound nuclei. The total neutron (proton) density is now considered to be composed of two parts:

- the core part $\rho_i^{\rm core}$,
- the tail part $\rho_i^{\rm tail}$,

so that $\rho_i(r) = \rho_i^{\rm core}(r) + \rho_i^{\rm tail}(r)$.

The core part of the density is taken to be [6]

$$\rho_i^{\rm core}(r) = \frac{\rho_i^0}{1 + \left[\frac{(1+(r/R)^2)}{2}\right]^{\beta_i} \left[e^{(r-R)/a_i} + e^{-(r+R)/a_i}\right]}. \tag{4}$$

The parameters $\rho_{\rm n}^0$ and $\rho_{\rm p}^0$ appearing in the expression of the density (eq. (4)) are fixed from the normalisation

$$4\pi \int \rho_{\rm n} r^2 {\rm d}r = N_{\rm c}, \tag{5}$$

$$4\pi \int \rho_{\rm p} r^2 {\rm d}r = Z, \tag{6}$$

where $N_{\rm c}$ (Z) is the total number of neutrons (protons) in the core nucleus. The only remaining parameter R is determined by requiring that the rms radius $r_{\rm p}$ of the proton density distribution (4) exactly reproduces the experimental rms charge radius $r_{\rm c}$, with

$$r_{\rm p} \approx (r_{\rm c}^2 - 0.64)^{1/2}. \tag{7}$$

The factor 0.64 accounts for the proton finite size.

The tail part of the density for the neutron-rich systems is given by [8]

$$\rho_{\rm tail} = N_0 \left(\frac{r^2}{(r^2 + R^2)^2}\right) \left(e^{r/a_t} + e^{-r/a_t}\right)^{-1}, \tag{8}$$

where

$$a_t = \frac{\hbar}{2(2m\varepsilon_t)^{1/2}}. \tag{9}$$

Here, ε_t is the neutron separation energy of the loosely bound nucleus (N, Z), while R, appearing in the expression of $\rho_{\rm tail}$, corresponds to the core nucleus $(N_{\rm c}, Z)$. The

Table 1. The separation energies and the proton mean-square-radii used in the present model calculations. The core and the tail parts used for loosely bound nuclei are also indicated in the last column.

Nucleus	$\varepsilon_{\rm p}$	$\varepsilon_{\rm n}$	$r_{\rm p}$	
^{20}Na	2.195	14.155	2.81	^{19}Ne + 1p
^{21}Na	2.431	17.100	2.86	^{19}F + 2p
^{22}Na	6.740	11.069	2.83	^{20}Na + 2n
^{23}Na	8.794	12.419	2.83	^{23}Na
^{24}Na	10.553	6.959	—	^{23}Na + 1n
^{25}Na	10.699	9.011	2.79	^{25}Na
^{26}Na	12.130	5.616	2.81	^{25}Na + 1n
^{27}Na	13.300	6.750	2.84	^{25}Na + 2n
^{28}Na	15.420	3.520	2.86	^{27}Na + 1n
^{29}Na	15.950	4.420	2.92	^{27}Na + 2n
^{30}Na	16.720	2.100	2.94	^{29}Na + 1n
^{31}Na	16.860	4.000	2.99	^{29}Na + 2n
^{32}Na	19.830	2.430	—	^{31}Na + 1n
^{33}Na	18.960	0.870	—	^{31}Na + 2n
^{12}C	15.957	18.722	2.34	^{12}C
^{19}F	7.994	10.432	2.79	^{19}F
^{19}Ne	6.411	11.639	2.78	^{19}Ne

constant N_0 is to be fixed by requiring that $\rho_{\rm tail}$ corresponds to the correct number of neutrons $(N - N_{\rm c})$ in the tail. For the proton density of (N, Z), we use the expression (eq. (4)) in which the proton separation energy $\varepsilon_{\rm p}$ and R correspond to the nucleus (N, Z) if the corresponding charge radius is available. This is supposed to take into account, approximately, the small differences in the proton distributions in the core $(N_{\rm c}, Z)$ and in the loosely bound nucleus (N, Z). If the charge radius of the loosely bound nucleus is not available, then the proton density for (N, Z) is taken to be same as that for the core nucleus $(N_{\rm c}$,$Z)$.

For the proton-rich nuclei we follow a similar procedure. The core part of the proton density is given by eq. (4), while the neutron density of (N, Z) is taken to be the same as that of the core nucleus $(N, Z_{\rm c})$. However, due to the different power behaviour, the proton tail is now taken to be

$$\rho_{\rm tail} = N_0 \left(\frac{r^2}{(r^2+R^2)^{2+q\alpha(\frac{mc^2}{(2\varepsilon_t)})^{1/2}}} \right) \left(e^{r/a_t} + e^{-r/a_t} \right)^{-1}. \quad (10)$$

Here a_t is given by the same expression (eq. (9)) as before except that ε_t (also appearing in eq. (10)) now corresponds to the proton separation energy of the loosely bound nucleus (N, Z).

It should be pointed out that the second exponential term e^{-r/a_t} (appearing in eq. (10)) was missing in [7]. The inclusion of this term only slightly modifies the final results, for example the extracted radii and the calculated cross-sections in the Glauber model change at most by two percent [8].

3 Results and discussion

We use the model discussed in the previous section for calculating the density distributions of the chain of sodium isotopes. The required input, namely the single neutron (proton) separation energies, $\varepsilon_{\rm n}$ ($\varepsilon_{\rm p}$), are taken from the compilation [16] and the experimental charge radii for the sodium nuclei are taken from [10]. Knowing the proton radius $r_{\rm p} = 2.83$ fm ($r_{\rm c} = 2.94$ fm [17]) of the stable sodium isotope, ^{23}Na, the charge radii of the remaining isotopes have been deduced from the isotopic shift measurements [9]. The single nucleon separation energies and the extracted proton radii [10] for the sodium chain are listed in table 1. We notice small single proton (neutron) separation energies for ^{20,21}Na (^{A} Na, $A = 28, 30, 32$ and 33), the proton- (neutron)-rich nuclei. The small separation energies play a crucial role in that they lead to thick nuclear skin or a halo. The core and the tail parts for individual isotopes used in the numerical calculations are explicitly shown in the last column of the same table. The separation energies taken from [16] and experimental charge radii from [17] for the target nucleus ^{12}C and the core nuclei (^{19}F and ^{19}Ne) are shown in the same table.

3.1 Density distributions

The model neutron and proton density distributions for representative cases, ^{23,27,31}Na, are shown in figs. 1, 2, 3, respectively. The core and the tail parts of the densities are explicitly shown. The corresponding density distributions of the RHB calculations [11] ($\rho_{\rm RHB}$) are also included in the figures for comparison.

It is to be pointed out that the proposed model density does not take into account the shell and deformation effects explicitly except through the use of observed single nucleon separation energies which are required as input.

It is also to be mentioned that the mean-field (both relativistic and non relativistic) calculations often yield small oscillations in the density at the center resulting in a small dip or bump in the density at the center. In the present work we are mainly concerned with the density in the surface and outer regions which are very important for loosely bound nuclei. Therefore, the differences between the model and RHB densities near the center are not discussed in the paper. In addition, these differences near the center are not sensitive to the reaction studies considered in this work.

The proton $(\rho(r)_{\rm p})$ and the neutron $(\rho(r)_{\rm n})$ densities of the present moddel are very similar for ^{23}Na (fig. 1) as expected. The same holds also for the corresponding RHB densities ($\rho_{\rm RHB}(r)_{\rm p}$ and $\rho_{\rm RHB}(r)_{\rm n}$). However, the model and the RHB densities differ at the surface. The model densities extend to larger distances as compared to those of RHB. The proton distributions $\rho(r)_{\rm p}$ and $\rho_{\rm RHB}(r)_{\rm p}$ are

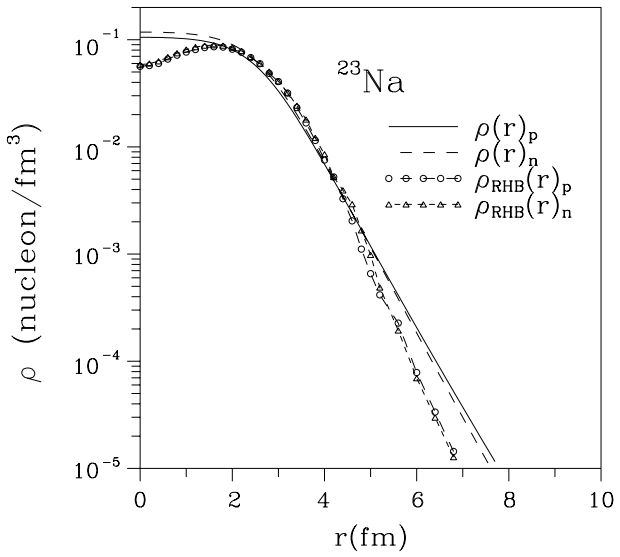

Fig. 1. The present model neutron and proton density distributions for ^{23}Na. The corresponding RHB distributions (see [11]) are also shown for comparison.

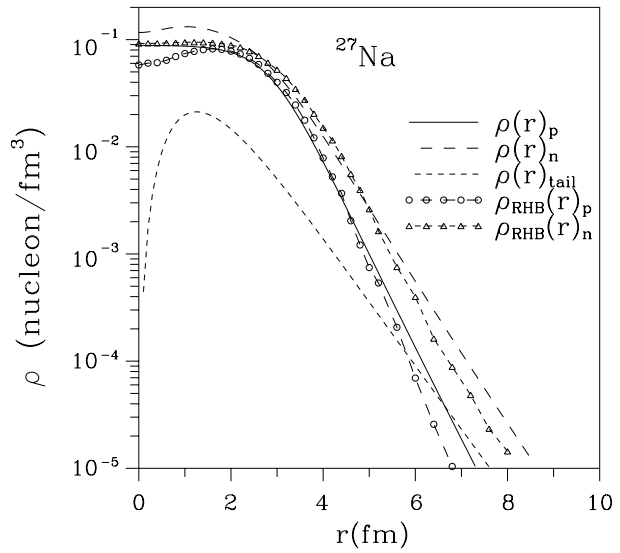

Fig. 2. The present model neutron and proton density distributions for ^{27}Na. The tail part ($\rho(r)_{\rm halo}$) is explicitly shown. The corresponding neutron and proton RHB distributions (see [11]) are also shown for comparison.

similar (fig. 2) for ^{27}Na with noticeable differences in the surface region. Similar remarks hold for the neutron density distributions presented in the same figure. However, the differences in the surface region now appear relatively earlier. The substantial contribution of the neutron tail at the surface in the model density is evident. Eventually at large r (asymptotic region) the total model density will merge, as required, with the tail. Similar observations hold for the density distributions of ^{31}Na (fig. 3), but the differences mentioned above are now much more enhanced. They appear even at smaller values of the radial distance r.

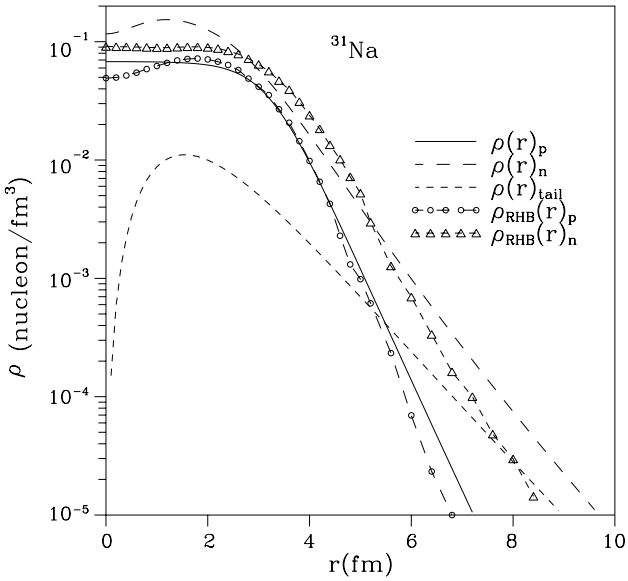

Fig. 3. The present model neutron and proton density distributions for ^{31}Na. The tail part ($\rho(r)_{\rm halo}$) is explicitly shown. The corresponding neutron and proton RHB distributions (see [11]) are also shown for comparison.

To summarize, the model density distributions differ from the corresponding RHB density distributions in the surface and outer regions. This is mainly because the present model has built-in correct asymptotic behaviour of the densities.

3.2 Radii

We now present and discuss the radii for the sodium isotopic chain. The model proton rms radii ($r_{\rm p}$ in fm) along with the corresponding RHB and the experimental values are shown in fig. 4. Clearly, the RHB results reproduce the experimental trend for neutron-rich isotopes (N $\geq$ 14). However, quantitatively the RHB values are lower for ^{30,31}Na. The RHB values considerably differ from the experiment for lighter sodium isotopes, in particular, large differences are noticed for ^{20}Na and ^{22}Na. At a finer level, the odd-even staggering, though very small, is visible throughout the chain. Similar results for the neutron rms radii ($r_{\rm n}$ in fm) are shown in fig. 5. The RHB results exhibit a monotonous increase in $r_{\rm n}$ with the neutron number, with very little odd-even staggering. The RHB results significantly differ from the experiment, particularly for ^{22}Na. In contrast, the model $r_{\rm n}$ are in perfect harmony with the corresponding experimental values throughout the chain.

One of the very interesting features of the loosely bound nuclei is the nuclear skin thickness ($r_{\rm n} - r_{\rm p}$). The variation of this skin thickness with mass number is shown in fig. 6 for the sodium chain. The RHB results show a steady increase in the skin thickness with the increase in the neutron number. Although these are qualitatively close to the corresponding experimental values, they do deviate from the experiment at various places, particularly

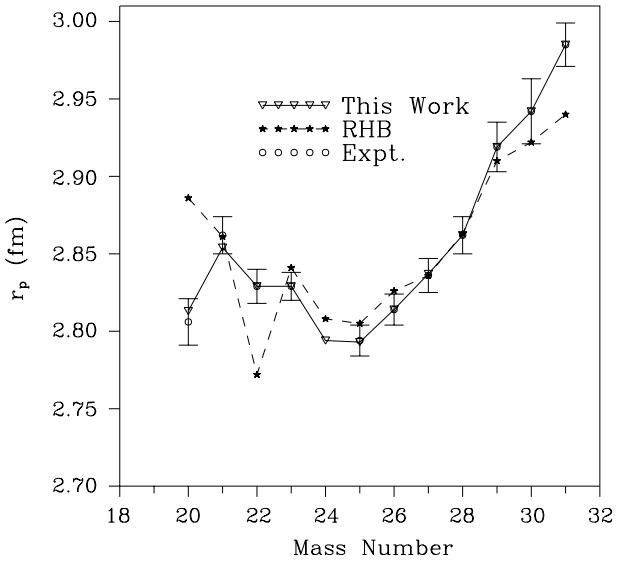

Fig. 4. The model rms proton radii for the chain of sodium isotopes. The corresponding experimental values taken from [10] and those obtained from RHB calculations (see [11]) are also included for comparison.

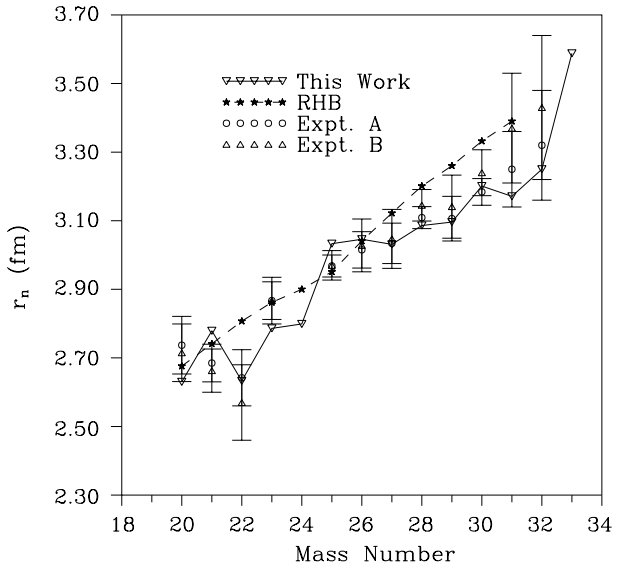

Fig. 5. The model rms neutron radii for the chain of sodium isotopes. The corresponding experimental values (Expt. A and Expt. B) taken from [10] and those obtained from RHB calculations (see [11]) are also shown for comparison.

for lighter isotopes. On the other hand, the skin thickness calculated using the model density is in perfect harmony with the experiment and reproduce the experimental values extremely well.

3.3 Cross-sections

The present model densities are used to calculate the reaction cross-sections σ_{R} for the sodium isotopes as projectiles (incident energy 950A MeV) on ^{12}C target within

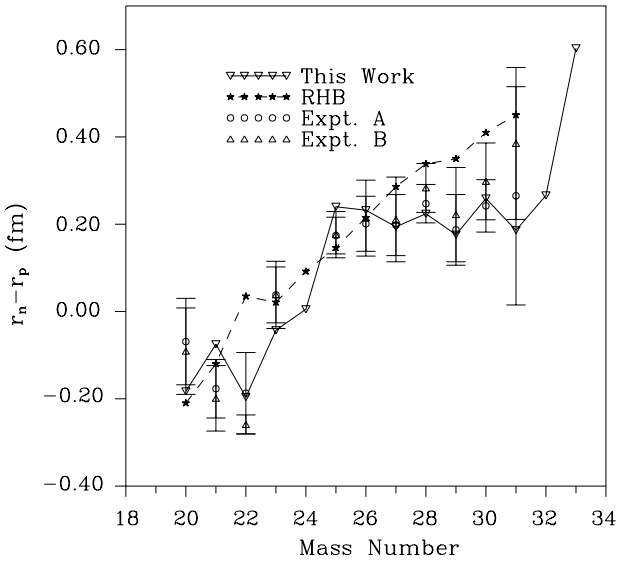

Fig. 6. The nuclear skin thickness ($r_{\mathrm{n}} - r_{\mathrm{p}}$), calculated using the present model densities, for the chain of sodium isotopes. The corresponding experimental values (Expt. A and Expt. B) extracted from those listed in [10] and the corresponding RHB values (see [11]) are also shown for comparison.

the Glauber model. The Glauber model requires neutron and proton densities of the target as well as of the projectile. In the numerical calculations, the required effective nucleon-nucleon cross-section is taken to be, following Tanihata [1], 0.8 times its free value at this energy. Explicitly, we use 46.99 (39.48) mb for the free value of p-p (p-n) cross-section at 790 MeV, the same as used by Tanihata [1].

3.3.1 Glauber model

The reaction cross-section σ_{R} in the Glauber model is given by

$$\sigma_{\mathrm{R}} = 2\pi \int \left[1 - T\left(b\right)\right] b \mathrm{d}b \,, \tag{11}$$

$T\left(b\right)$ is the Transparency function at impact parameter b. The nucleon profile function is replaced by average NN cross-section $\overline{\sigma}$ in the optical limit approximation. In the zero range limit, the transparency function $T\left(b\right)$ becomes

$$T\left(b\right) = \exp\left[-\overline{\sigma} \int \mathrm{d}s \overline{\rho}_{\mathrm{t}}\left(s\right) \overline{\rho}_{\mathrm{p}}\left(\mathbf{b} - \mathbf{s}\right)\right]. \tag{12}$$

The suffixes t and p stand for target and projectile, respectively. $\overline{\rho}_i\left(s\right)$ is a z-direction integrated nucleon (sum of neutron and proton) density distribution expressed as

$$\overline{\rho}_i\left(s\right) = \int \mathrm{d}z \rho\left(\sqrt{s^2 + z^2}\right) , \tag{13}$$

with $s^2 = \left(x^2 + y^2\right)$. Thus the calculation of the reaction cross-section in this model requires the average NN cross-section and the density distributions of both the target and the projectile.

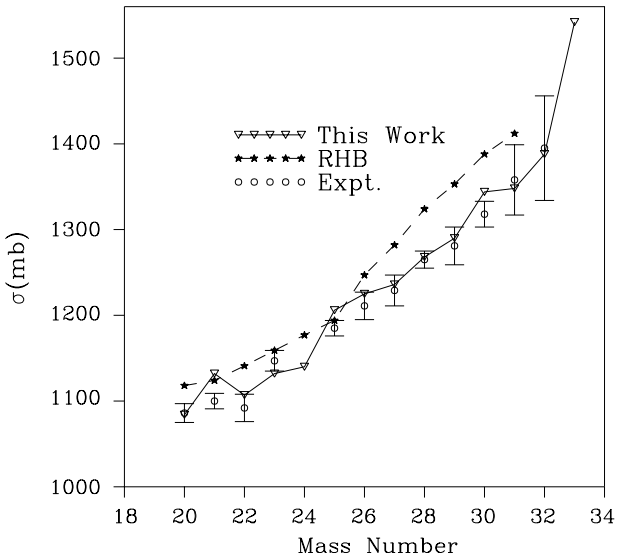

Fig. 7. The interaction cross-sections calculated by using the present model densities, in the Glauber model, for sodium isotopes as projectiles incident on ^{12}C target at 950A MeV. The corresponding experimental (see [10]) and the RHB results (see [12]) are also included for comparison.

It is worth mentioning that the work of the Surrey group [18] shows that the inclusion of the few-body structure of the loosely bound projectiles (like ^{8}B, ^{11}Li and ^{11}Be) and the adiabatic nature of the projectile-target interaction, in the Glauber model, leads to slightly larger values of the extracted neutron radii of the projectiles.

3.3.2 Results

The calculated Glauber cross-sections using the model densities, along with the available experimental values are presented in fig. 7. Similar results obtained with RHB densities are also shown for comparison. The present model calculation and the corresponding RHB results reproduce the experimental trend (monotonous increase with the neutron number) for the heavier isotopes of the chain. However, the RHB results overestimate the cross-sections. For the lighter isotopes ($^{20\text{-}22}$Na), there exist small differences between the RHB and the experimental results. The present model calculations are in better agreement with the experiment, throughout, both in magnitude as well as in the systematics.

4 Conclusions

The neutron and proton density distributions for the chain of sodium isotopes are investigated using the semi-phenomenological nucleon density model. The model incorporates correctly the asymptotic behaviour and the behaviour near the centre, both for the core and the tail parts of the density. The single nucleon (neutron and proton) separation energies and the charge radii are required as input information in the explicit calculations. These are taken from the experiment. The model density distributions, radii and nuclear skin thickness are compared with the corresponding Relativistic Hartree-Bogoliubov (RHB) results and also with the experiment. The model density distributions qualitatively agree with those of RHB, the differences do appear especially at the surface. The model distributions extend to larger distances. This is mainly due to the correct built-in asymptotic behaviour in the density model. The RHB radii and cross-sections, though, are in qualitative agreement with the experiment, deviations are noticed in several cases. On the other hand, the radii, skin thickness and cross-sections, obtained by using the model densities, are found to be in almost perfect harmony with the experiment. It can then be concluded that the present semi-phenomenological model density gives a fair representation of the nucleon (neutron and proton) densities in the stable as well as in the loosely bound nuclei.

Two of us (YKG and AB) are thankful to S.H. Patil for his valuable suggestions and discussions. One of us (YKG) acknowledges the partial financial support from the French Ministère de la Recherche and the hospitality of the Institut de Physique Nucléaire at Orsay where part of this work was performed. The financial support from the Department of Science and Technology (DST), Government of India (proj. no. SP/S2/K-04/99) is gratefully acknowledged.

References

1. I. Tanihata *et. al.*, Phys. Rev. Lett. **55**, 2676 (1985).
2. I. Tanihata, J. Phys. G **22**, 157 (1996); Prog. Part. Nucl. Phys. **35**, 505 (1995).
3. C.J. Betty *et. al.* Adv. Nucl. Phys. **19**, 1 (1989); T. Suzuki, Phys. Rev. C **45**, 1939 (1992); T. Suzuki *et. al.*, Phys. Rev. C **50**, 2815 (1994), and references therein.
4. I. Tanihata *et. al.*, Phys. Lett. B **206**, 592 (1988).
5. I. Tanihata *et. al.*, Phys. Lett. B **287**, 307 (1992).
6. Y.K. Gambhir, S.H. Patil, Z. Phys. A **321**, 161 (1985), Z. Phys. A **324**, 9 (1986).
7. A. Bhagwat, Y.K. Gambhir, S.H. Patil, Eur. Phys. J. A **8**, 511 (2000).
8. A. Bhagwat, Y.K. Gambhir, S.H. Patil, J. Phys. G **27**, B1 (2001).
9. G. Huber *et. al.*, Phys. Rev. C **18**, 2342 (1978).
10. T. Suzuki *et. al.*, Phys. Rev. Lett. **75**, 3241 (1995), Nucl. Phys. A **616**, 286c (1997).
11. G.A. Lalazissis, D. Vretenar, W. Pöschl, P. Ring, Nucl. Phys. A **632**, 363 (1998).
12. J. Meng, I. Tanihata, S. Yamaji, Phys. Lett. B **419**, 1 (1998).
13. J. Dobaczewski, Acta Phys. Polonica B **30**, 1647 (1999).
14. G.A. Lalazissis *et. al.*, Z. Phys. A **357**, 429 (1997).
15. Y.K. Gambhir, P. Ring, H. De Vries, Europhys. Lett. **10**, 219 (1989).
16. G. Audi, A.H. Wapstra, Nucl. Phys. A **565**, 1; 66 (1993).
17. C.W. de Jager, H. de Vries, C. de Vries, At. Data Nucl. Data Tables **36**, 495 (1987); **565**, 66 (1993).
18. Al-Khalili *et. al.*, Phys. Rev. Lett. **76**, 3903 (1996).